Lateral current injection photonic crystal membrane light emitting diodes

Christopher M. Long,[a] Antonios V. Giannopoulos, and Kent D. Choquette[b]
Department of Electrical and Computer Engineering, University of Illinois, 208 N. Wright St., Urbana, Illinois 61801

A novel method for fabricating photonic crystal membrane light emitting diodes is presented. The device employs a transverse diode structure and injects carriers laterally through a photonic crystal patterned at the *p-n* junction within a membrane. Details of the fabrication process as well as electrical and optical characteristics of the devices are presented. © *2010 American Vacuum Society.* [DOI: 10.1116/1.3360891]

I. INTRODUCTION

Photonic crystals (PhCs) have enabled new opportunities to control light at the wavelength scale. This characteristic has been exploited in many ways, creating ultrasmall lasers,[1,2] band edge lasers,[3] and cavities with extremely high quality factors.[4] PhCs are usually excited optically by using microphotoluminescence or evanescent fiber coupling. This has been sufficient in characterizing and developing PhC applications, but ultimately, electrical excitation of PhCs will be necessary before they can find widespread usage. There are a few examples of electrically injected PhC light emitters,[5–8] with structures designed to allow electrical injection, provide adequate heat sinking, and minimize optical loss. These are difficult constraints to satisfy simultaneously, therefore fabrication has been a delicate procedure, at times requiring intricate wet etches,[5] wafer fusion,[6] air bridge contacts,[7] multiple electron beam lithography iterations,[7,8] and epitaxial regrowth.[8] A robust fabrication process is necessary to create electrically injected PhC emitters that still maintain the exceptional qualities found with optically pumped devices. To meet this need, the devices described herein make use of lateral current injection (LCI),[9–12] whereby a transverse diode is first created within a semiconductor membrane via ion implantation doping, followed by patterning of a PhC at the diode junction (Fig. 1). This process offers advantages over vertically injected PhC emitters, including greater freedom in the choice of PhC pattern and reduced fabrication complexity. More generally, LCI allows for independent control and arbitrary location, enabling passive and active device integrations important for new applications, such as optoelectronic integrated circuits[13] and resonant sensor arrays. The design, fabrication, and characterization of LCI PhC emitters fabricated in InP-based semiconductors are described.

II. PHOTONIC CRYSTAL DESIGN

A PhC is composed of a lattice of high and low optical index materials with a period that is approximately equal to the wavelength of light. An electromagnetic wave propagating within the PhC will interact strongly with the lattice, giving rise to variable optical dispersion within the material that can be altered by design of the lattice geometry and choice of optical material. PhCs are often fabricated as a quasi-two-dimensional structure, with the lattice created in a thin membrane of semiconductor material.[1] The membrane acts as a slab waveguide and confines the light within the membrane via total internal reflection. Using a membrane and a two-dimensional PhC avoids the complicated procedures required to create a full three-dimensional structure, and allows the use of established, planar microfabrication techniques.

The choice of PhC is an important aspect of a successful electrically injected PhC diode. A membrane PhC, with its narrow veins of semiconductor material between its holes and relatively thin slab, has inherently poor electrical conduction, so optimization is needed. A first parameter to consider is efficient carrier injection: The PhC design must support low-resistance current paths with minimal nonradiative recombination centers. Second, there must be adequate heat sinking within the structure. Gain and loss within a semiconductor are very sensitive to device temperature so efficient pathways to sufficiently cool the device are required. Finally, the modified PhC must support and confine electromagnetic modes. The most direct way to improve carrier transport is to reduce the density of etched air holes in the photonic crystal. This will increase the semiconductor current paths, reduce nonradiative surface recombination, and allow for more efficient heat transfer out of the lattice. Hole deletions can be done periodically within a triangular lattice, thus transforming it into a graphene or kagome lattice.[14,15]

This article describes the electrical and spectral properties of an electrically injected PhC with a homogeneous graphene lattice that contains 28×31 unit cells. The photonic band diagram for the graphene lattice is provided in Fig. 2, showing that it possesses a photonic band gap and a flat (slow light) band. The device supports nonlocalized Bloch modes that can be excited at an arbitrary location within the crystal. The main advantage of a graphene lattice over other PhC patterns (kagome, triangular) is that it possesses a slow light band at the edge of the photonic band gap. Slow light bands have been shown to form more quickly in finite-sized lattices

[a] Present address: School of Electrical and Computer Engineering, Purdue University, 465 Northwestern Ave., West Lafayette, Indiana 47907.
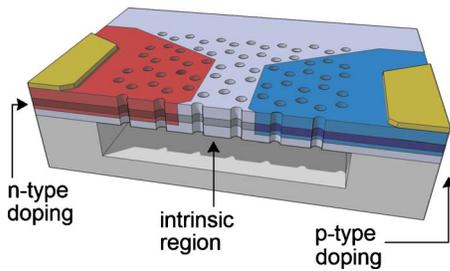[b] Electronic mail: choquett@uiuc.edu

FIG. 1. (Color online) Schematic of the LCI PhC emitter with a graphene-type bulk PhC.

TABLE I. Epitaxial structure for the wafer used to create the LCI PhC emitter.

Thickness (nm)	Material
100	InP
57.5	1.1Q InGaAsP
30	1.2Q InGaAsP
5.5×6	1.55Q InGaAsP
17×5	1.2Q InGaAsP
30	1.2Q InGaAsP
57.5	1.1Q InGaAsP
1000	InP

than is the case for band edge states;[16] therefore it is expected that photonic crystal effects will be evidenced in relatively small lattices.

III. DEVICE FABRICATION

The LCI PhC emitters are fabricated in an undoped 280 nm membrane of InGaAsP quaternary semiconductor material that is designed to balance the optical and electrical requirements of a PhC emitter (see Table I). There are six strain-compensated quantum wells that are designed to emit with a peak wavelength of 1550 nm. It is epitaxially grown on an undoped InP substrate and buried under a 100 nm sacrificial layer of InP. The outermost epitaxial layers of the membrane consist of wider-band gap semiconductors that help confine current to the center of the membrane. The total membrane thickness (approximately 0.6λ) is increased to maximize the cross-sectional area of the current channel and so reduce the electrical resistance while still maintaining the single-mode cutoff condition of the slab.[17]

The transverse diode structure is created by ion implantation doping. Ion implantation offers precise spatial control of the dopants and provides a method to selectively tune the semiconductor band gap through quantum well intermixing.[18] For this step, a masking layer of SiN (1 μm) is deposited onto the sample with plasma enhanced chemical vapor deposition (PECVD) and patterned using photoresist
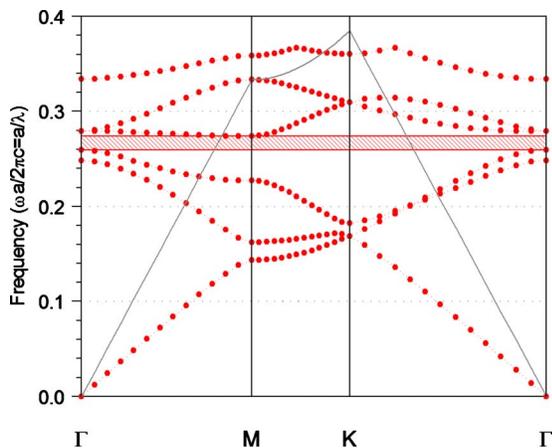

FIG. 2. (Color online) Photonic band diagram for the graphene lattice. Modal frequencies have been normalized to the nearest neighbor distance a. The calculation uses $a = 400$ nm and hole radii of $r = 0.31a$.

and Freon-14 reactive ion etch (RIE). The implantation schedule[19] is designed to uniformly dope the n-type regions of the membrane with Si to a concentration of $5 \times 10^{18}/cm^3$. The sample is heated to 200 °C during implantation in order to mitigate implantation damage and improve the electrical properties of the semiconductor.[19,20] Following implantation, the SiN mask is removed and another SiN layer is deposited. New areas of the mask are etched away to expose the regions of the diodes for p-type doping. The sample is coimplanted with Be and P ions to a concentration of $5 \times 10^{18}/cm^3$. Coimplantation with P creates excess crystal damage to decrease Be diffusion and increase dopant activation and carrier mobility.[21]

The implantation process creates defects within the InGaAsP material, which can be annealed with high temperature processing. Heating also allows the dopant atoms to become electrically active. The sample is annealed at 800 °C for 5 s. During this process, a thin cap layer of SiN is first deposited onto the sample and it is placed face-down on a piece of InP to prevent outdiffusion of P at high temperature.[22] Annealing the sample at high temperatures also intermixes the various epitaxial layers within the membrane. This has an affect of homogenizing the membrane and therefore increasing the band gap energy within the semiconductor quantum well as atoms from the barrier regions diffuse into the well. Quantum well intermixing is enhanced when defects are introduced to the crystalline structure. This process can be used to vary the energy gap to increase carrier confinement and reduce optical loss. When carriers are injected into the intrinsic region of the diode structure, a fraction of the population will traverse across the diode and recombine in the doped region. An intermixed higher band gap in the region surrounding the PhC creates lateral energy barriers, increasing the carrier density and, therefore, increasing the gain within the PhC region. Previous studies have shown a substantial decrease in transverse junction laser threshold by the addition of lateral energy barriers.[23] A second advantage of increasing the band gap is to reduce absorptive loss in the region surrounding the intrinsic region.[24]

Metal layers of AuGe/Ni/Au are deposited to contact to the n-doped regions[25] of the device using standard liftoff techniques. This is followed by lift-off of AuBe/Au layers to contact to the p-doped regions.[26] The metal is sintered at
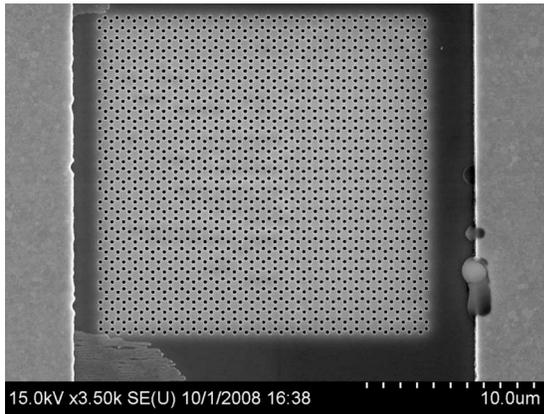
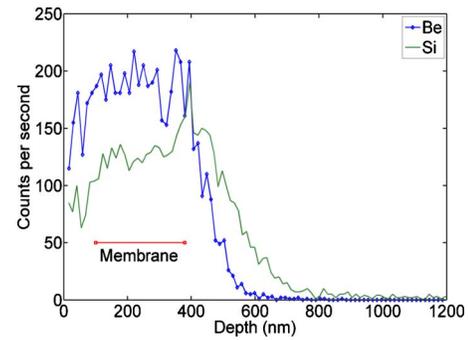FIG. 3. Scanning electron micrograph image of the graphene LCI PhC.

FIG. 4. (Color online) Dopant profile for Si and Be obtained via SIMS measurement. Values along the y axis correspond linearly to actual concentration values.

400 °C for 30 s to form low-resistance contacts with the material. A layer of SiO_2 to be used as an etch mask is deposited onto the sample using PECVD. This is followed by spinning on a layer of polymethylmethacrylate (PMMA) electron beam resist. PhC designs are patterned into the PMMA using a JEOL JBX-6000FS electron beam lithography system. The patterns are transferred into the SiO_2 by Freon-23 RIE and the remaining PMMA is stripped from the sample. The photonic crystals are etched into the sample using a PlasmaTherm SLR-770 inductively coupled plasma reactive ion etcher (ICP-RIE). High quality devices require vertical holes with low surface roughness,[27] but this will only occur if the different layers of InGaAsP compounds etch at similar rates. It was found that a balance between Cl, H, and Ar will generate a similar etch rate between the different materials.[28] After ICP-RIE, the sacrificial InP layers are removed via a room-temperature wet etch with a mixture of hydrochloric and phosphoric acids.[29] A scanning electron microscope image of the completed device is shown in Fig. 3.

IV. DEVICE CHARACTERIZATION

The LCI PhC emitter is characterized with and without PhC patterns to elucidate how the fabrication process affects the optical and electrical properties of the device.

A. Implantation characterization

The relative impurity concentrations are measured using secondary ion mass spectroscopy (SIMS) and are shown in Fig. 4. The element profiles in Fig. 4 indicate that the membrane structure is doped to the desired depth, although the absolute impurity concentration has not been calibrated. The spatial selectivity of the ion implantation is measured using stripes that had been patterned into the SiN implantation mask. The stripes vary in thickness from 2 to 15 μm, with a separation between stripes equal to the stripe width. Because of lateral straggle during implantation and diffusion, there will be a limit to the smallest features that can be defined with ion implantation. Areas that are protected from the implantation will emit a spectrum identical to the unprocessed sample, while areas that are subjected to implantation will

emit at a shorter wavelength due to quantum well intermixing, or not at all due to crystal damage. A minimum spatial resolution of 2.5 μm was measured for the p-doped region and 1.5 μm in the n-doped region, indicating that the diodes designed to have an intrinsic region less than 4 μm will have overlap between the n- and p-doped regions.

The effects of quantum well intermixing are examined with microphotoluminescence. The spectrum from an unprocessed sample is presented in Fig. 5 alongside spectra from the intrinsic (no implantation, but annealed), p- and n-doped regions of the completed sample. The peak emission wavelengths from these regions have shifted to 1467, 1352, and 1310 nm, respectively, from the initial peak wavelength of 1550 nm. The lateral energy barrier around the intrinsic region created by intermixing is 71 meV at the p-doped side and 101 meV at the n-doped side, with band offsets estimated at 60% in the valence band and 40% in the conduction band. The decreased radiative efficiency in the doped regions in Fig. 5, especially in the n-type areas, is due to residual implantation damage that remains after annealing.
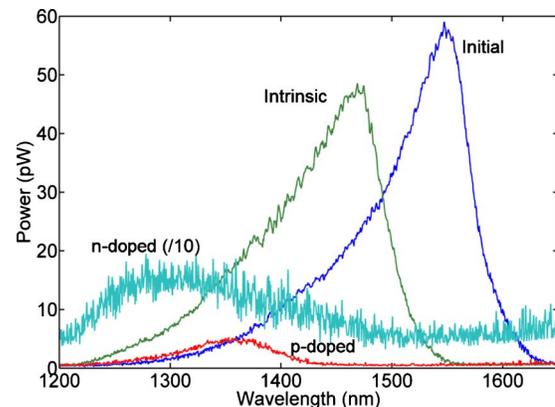

FIG. 5. (Color online) Microphotoluminescence spectra of a sample before and after undergoing implantation and anneal. The peak emission wavelength shifts and output power decreases by varying amounts due to implantation effects. Spectrum for n-doped region has been increased by ten times.

FIG. 7. (Color online) EL spectra of a bulk graphene PhC for various lattice constants. The device is excited by 15 V pulses with 35% duty cycle and 100 ns pulse width.
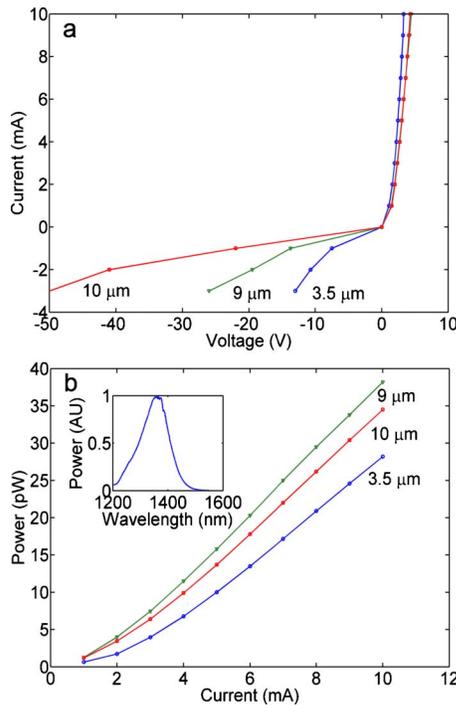
FIG. 6. (Color online) (a) Current-voltage curve and (b) current-light curve for laterally injected light emitting diodes as a function of nominal diode width. Inset: a typical EL spectrum from an unpatterned LCI diode.

B. Electrical characterization

The device resistivity is characterized via transfer length measurements,[30] which indicate a contact resistance of 8 Ω (120 Ω) for the n-type (p-type) contact and a sheet resistance of 230 $\Omega/\square$ (1480 $\Omega/\square$) for the n-doped (p-doped) regions. These values are similar to the results found in Ref. 21. A series of lateral diodes are created to study the effect of separation between the n- and p-doped regions. Figure 6(a) shows selected examples of the current-voltage (IV) curve of a lateral diode as a function of nominal junction width. All devices possess a forward differential resistance of approximately 300 Ω, but the reverse bias characteristics are more variable.

Current density is estimated for LCI diodes using the piecewise linear model, where the diode is modeled as a voltage source in series with a resistor. Because the implanted region connecting the metal contact to the p-n junction is trapezoidal (see Fig. 1), the diode resistance will vary according to the current path. To account for this, the diode is divided into 1×1 μm^2 squares, and each square is assigned a resistance value. The resistance of one row of squares that spans from one metal contact across junction to the opposite metal contact is found as the weighted sum of the square regions within the row. The total resistance for the diode is calculated by adding the resistances of the rows as resistors in parallel.

The sheet resistances of the doped regions were measured as discussed above; since no measurement of the resistivity of the intrinsic region is available, it is used as a fitting parameter to match the measured overall diode differential
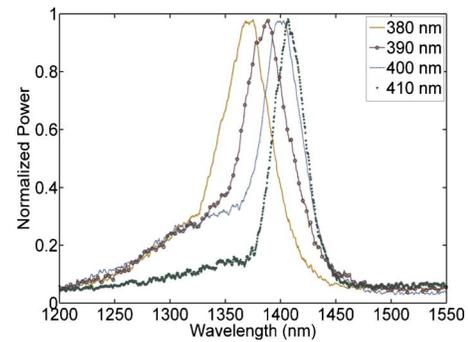
resistance. By modeling a device with an intrinsic region span of 2 μm, a derived value of 1400 $\Omega/\square$ for the intrinsic region arises from the total differential resistance of 300 Ω. This relatively low value for the intrinsic region resistivity is attributed to unintentional doping of the semiconductor membrane during growth. The offset voltage (diode built-in voltage) is estimated to be 1.3 V from the IV curve in Fig. 6(a), which is close to the calculated contact potential of 1.1 V. In order to estimate the current density, we assume that all current conduction takes place within 1 μm of the sample surface and that none is lost to recombination currents. A forward bias of 10 mA produces a current density of 14 kA/cm^2 in the middle of the diode and 9 kA/cm^2 at the edges of the diode, with estimated resultant carrier concentrations of 3×10^{18} and 2×10^{18} cm^{-3}, respectively. These values represent a best-case scenario for current density; nonradiative recombination and current shunt paths will significantly reduce these values.

C. Optical characterization

A lensed multimode fiber is placed directly above the diodes and positioned such that it maximizes the power coupled into the fiber. The optical power is recorded as a function of input current and plotted in Fig. 6(b) for the same devices as Fig. 6(a). The output power is linear for injection currents above 1 mA and approximately scales with the size of the intrinsic region.

The electroluminescence (EL) spectrum of the complete LCI PhC is shown in Fig. 7 and indicates that the emission is dominated by a single PhC resonance that varies from 1370 to 1410 nm depending on the PhC period, and corresponds to emission from the slow light band directly above the photonic band gap[31] shown in Fig. 2. The modified spontaneous emission[31] stems from two important characteristics within these devices: an increase in the photonic density of states that accompanies flat photonic bands and a trapping of charge carriers due to inhibited recombination in the photonic band gap. Furthermore, it is the presence of the slow light band, rather than a band edge, that is key to enabling this enhancement; this is exemplified when trying to excite band edge modes in the PhC. By examining other samples with
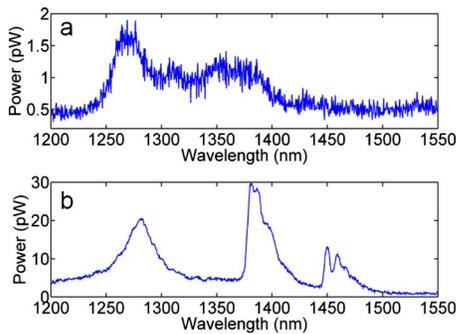
FIG. 8. (Color online) (a) EL spectrum for a bulk graphene PhC with a lattice constant of 350 nm. (b) The microphotoluminescence spectrum for the same device exhibiting emission from multiple PhC resonances.

different lattice constants, the quantum well gain is brought into resonance with other PhC modes. For example, the EL spectrum from a device with a lattice constant of 350 nm shows weak (gain-limited) emission into a band edge mode [Fig. 8(a)] despite the fact that optical excitation displays strong emission into three distinct modes [Fig. 8(b)].

The optical spectra are measured as a function of position within the lateral diode, as shown in Fig. 9. The diodes are biased at 7 mA dc and then spectra are taken at locations spaced 2 μm across the diode, with the first spectrum measured at the edge of the metal contact to the p-doped region (0 μm in Fig. 9) and the last at the metal contact to the n-doped region (25 μm in Fig. 9). Figure 9(a) shows the result for a diode without an etched PhC pattern. The emission increases starting near the edge of the p-type contact and reaches its maximum at a distance 10 μm from the edge of the metal. Beyond 13 μm, the emission rapidly decreases primarily because of residual implantation damage in the n-doped region, but the hole diffusion length also plays a role. Figure 9(b) shows the emission spectra from a bulk graphene PhC in a similarly sized lateral diode, biased at 7 mA dc. At the left hand side of the plot, the diode displays broad quantum well emission, similar to Fig. 9(a). At a distance of 10–15 μm from the p-type contact, the emission becomes sharply peaked at 1375 nm because of the influence of the PhC. For distances greater than 15 μm, the emission

power declines and the resonance shifts to a shorter wavelength. As shown below, this shift is consistent with the expected shift produced by edge effects of the PhC.

V. ANALYSIS

The EL behavior of the LCI PhCs shows preferential emission into slow light bands and a resonance shift at the edges of the PhC. These characteristics are consistent with the results of a two-dimensional finite-difference time-domain simulation of a large graphene lattice. Graphene PhCs with different numbers of unit cells are laid out using commercial simulation software. A source is placed near the middle of the PhC lattice that excites the PhC with an input pulse that is centered spectrally at 1325 nm. Time monitors sample the electromagnetic field at various locations in the PhC, and after the simulation runs 65536 time steps, the frequency spectrum is calculated as the Fourier transform of the sampled field, as shown in Fig. 10. The spectrum for the largest PhC (11×13 unit cells) is well developed in Fig. 10(a), and shows sharp resonances at 1.26, 1.37, and 1.46 μm, and a band gap that spans 0.1 μm. The two closely spaced resonances marked by the arrow in Fig. 10(a) at 1.25 and 1.27 μm come from the Γ and M symmetry points of the fourth band shown in Fig. 2, and there is a range of emitted power from the slow light band in between. When the number of cells is reduced to 5×5 in Fig. 10(b), the peak at 1.25 μm broadens, indicating lower quality factor for this mode, and the peaks at 1.37 and 1.46 μm disappear. Remarkably, a graphene PhC with just 2×3 unit cells will still support the shortest-wavelength modes, as apparent in Fig. 10(c). In this case, however, the mode has moved to a shorter wavelength and is now resonant at 1.24 μm. Similar observations have been noted for Γ-point modes in hexagonal lattices.[32] These simulations show that certain modes are more likely to form in smaller lattices, and suggest that the large PhC lattices in the fabricated devices are adversely affected by optical loss, causing them to behave like much smaller PhCs.

VI. CONCLUSION

The spectral and electrical properties of laterally injected PhC light emitting diodes are presented. This work is a new approach to the creation of PhC emitters that aims to be more robust and less complicated than other fabrication methods. These devices are monolithic and require only a single iteration of electron beam lithography, and so their fabrication complexity is similar to that required for photopumped devices. The devices herein take advantage of PhC designs that increase their electrical and radiative efficiency, and post-growth band gap engineering to enhance lateral carrier confinement and limit optical loss. These optimizations produce spontaneous EL emission with spectral properties that are modified by the PhC, showing enhanced radiation from the slow light mode of the PhC and inhibited radiation due to the photonic band gap. The measurements are shown to be consistent with predicted results from electromagnetic
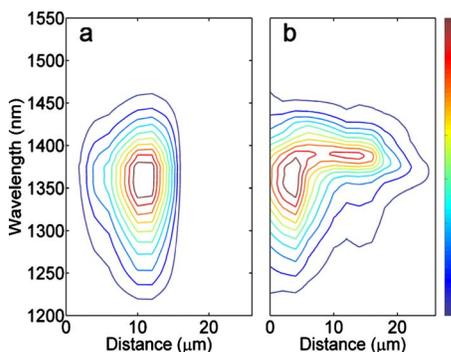

FIG. 9. (Color online) Contour plots of the EL emission spectra as a function of location within the diode for (a) a blank diode and (b) a bulk graphene PhC. Both devices are biased at 7 mA dc.
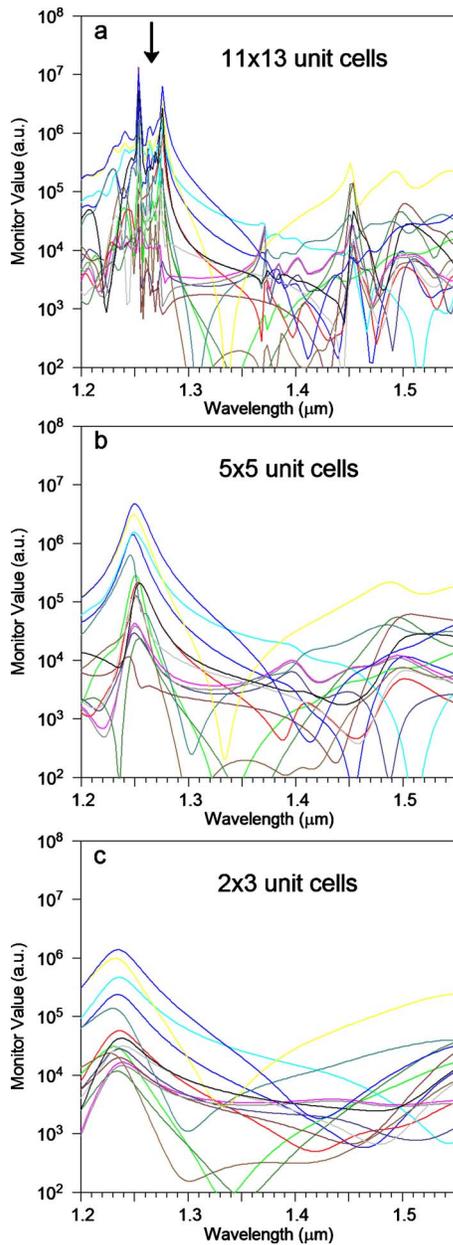
FIG. 10. (Color online) Simulated spectra for a graphene lattice with different numbers of unit cells. The resonant mode seen in electroluminescent characterization (Fig. 7) is indicated by arrows in the spectrum from the largest PhC.

simulations. The estimated carrier concentrations obtained at the lateral junction are found to be relatively low, and stimulated emission has not been observed. Parasitic current shunt paths, such as through the undoped substrate, are suspected to limit the optical gain. Further work is necessary to improve the carrier injection efficiency to increase the carrier concentrations to produce a LCI PhC laser.

[1] O. Painter, R. K. Lee, A. Sherer, A. Yariv, J. D. O'Brien, P. D. Dapkus, and I. Kim, Science **284**, 1819 (1999).
[2] Z. Zhang and M. Qiu, Opt. Express **12**, 3988 (2004).
[3] H. Y. Ryu, S. H. Kwon, Y. J. Lee, Y. H. Lee, and J. S. Kim, Appl. Phys. Lett. **80**, 3476 (2002).
[4] B. S. Song, S. Noda, T. Asano, and Y. Akahane, Nature Mater. **4**, 207 (2005).
[5] H. G. Park, S. H. Kim, M. K. Seo, Y. G. Ju, S. B. Kim, and Y. H. Lee, IEEE J. Quantum Electron. **41**, 1131 (2005).
[6] M. Imada, S. Noda, A. Chutinan, T. Tokuda, M. Murata, and G. Sasaki, Appl. Phys. Lett. **75**, 316 (1999).
[7] S. Chakravarty, P. Bhattacharya, and Z. Mi, IEEE Photonics Technol. Lett. **18**, 2665 (2006).
[8] Y. K. Kim, V. C. Elarde, C. M. Long, J. J. Coleman, and K. D. Choquette, J. Appl. Phys. **104**, 123103 (2008).
[9] H. Namizaki, H. Kan, M. Ishii, and A. Ito, J. Appl. Phys. **45**, 2785 (1974).
[10] K. Oe, Y. Noguchi, and C. Caneau, IEEE Photonics Technol. Lett. **6**, 479 (1994).
[11] A. A. Tager, R. Gaska, I. A. Avrutsky, M. Fay, H. Chik, A. SpringThorpe, S. Eicher, J. M. Xu, and M. Shur, IEEE J. Sel. Top. Quantum Electron. **5**, 664 (1999).
[12] C. F. Schaus, A. J. Torres, J. Cheng, S. Sun, C. Hains, K. J. Malloy, H. E. Schaus, E. A. Armour, and K. Zheng, Appl. Phys. Lett. **58**, 1736 (1991).
[13] S. Charbonneau *et al.*, IEEE J. Sel. Top. Quantum Electron. **4**, 772 (1998).
[14] J. Mouette *et al.*, Electron. Lett. **39**, 526 (2003).
[15] A. V. Giannopoulos, C. M. Long, and K. D. Choquette, Electron. Lett. **44**, 803 (2008).
[16] K. Sakoda, *Optical Properties of Photonic Crystals* (Springer, Berlin, 2005), pp. 187–191.
[17] S. G. Johnson, S. Fan, P. R. Villeneuve, and J. D. Joannopoulos, Phys. Rev. B **60**, 5751 (1999).
[18] P. Gavrilovic, D. G. Deppe, K. Meehan, J. N. Holonyak, J. J. Coleman, and R. D. Burnham, Appl. Phys. Lett. **47**, 130 (1985).
[19] B. J. Sealy, in *Properties, Processing and Applications of Indium Phosphide*, edited by T. P. Pearsall (IEEE, London, 2000), pp. 231–245.
[20] S. Charbonneau *et al.*, J. Appl. Phys. **78**, 3697 (1995).
[21] M. V. Rao and R. K. Nadella, J. Appl. Phys. **67**, 1761 (1990).
[22] S. J. Pearton and A. Katz, Mater. Sci. Eng., B **18**, 153 (1993).
[23] E. H. Sargent, G. L. Tan, and J. M. Xu, IEEE J. Sel. Top. Quantum Electron. **3**, 507 (1997).
[24] J. J. He, E. S. Koteles, P. J. Poole, M. Davies, R. Goldberg, I. Mitchell, and S. Charbonneau, Electron. Lett. **31**, 2094 (1995).
[25] A. G. Baca, F. Ren, J. C. Zolper, R. D. Briggs, and S. J. Pearton, Thin Solid Films **308–309**, 599 (1997).
[26] A. Katz, Proc. SPIE **1393**, 67 (1991).
[27] T. Asano, B.-S. Song, and S. Noda, Opt. Express **14**, 1996 (2006).
[28] S. L. Rommel *et al.*, J. Vac. Sci. Technol. B **20**, 1327 (2002).
[29] S. B. Phatak and G. Kelner, J. Electrochem. Soc. **126**, 287 (1979).
[30] D. K. Schroder, *Semiconductor Material and Device Characterization*, 3rd ed. (Wiley, Hoboken, 2006), pp. 146–148.
[31] C. M. Long, A. V. Giannopoulos, and K. D. Choquette, Electron. Lett. **45**, 227 (2009).
[32] H. Y. Ryu, M. Notomi, and Y. H. Lee, Phys. Rev. B **68**, 045209 (2003).